ACS APPLIED MATERIALS & INTERFACES

Research Article

www.acsami.org

Biocompatible Slippery Fluid-Infused Films Composed of Chitosan and Alginate via Layer-by-Layer Self-Assembly and Their Antithrombogenicity

Kengo Manabe, Kyu-Hong Kyung, and Seimei Shiratori*

Department of Applied Physics and Physico-Informatics, Faculty of Science and Technology, Keio University, 3-14-1 Hiyoshi, Kohoku-ku, Yokohama, Kanagawa 223-8522, Japan

Supporting Information

ABSTRACT: Antifouling super-repellent surfaces inspired by *Nepenthes*, the pitcher plant, were designed and named slippery liquid-infused porous surfaces (SLIPS). These surfaces repel various simple and complex liquids including water and blood by maintaining a low sliding angle. Previous studies have reported the development of fluorinated SLIPS that are not biocompatible. Here, we fabricated fluid-infused films composed of biodegradable materials and a biocompatible lubricant liquid. The film was constructed using a combination of electrostatic interactions between chitosan and alginate and hydrogen-bonding between alginate and polyvinylpyrrolidone (PVPON) via the layer-by-layer self-assembly method. After chitosan and alginate were cross-linked, the PVPON was removed by increasing the pH to generate porosity from the deconstruction of the hydrogen-bonding. The porous underlayer was hydrophobized and covered by biocompatible almond oil. Blood easily flowed over this biodegradable and biocompatible SLIPS without leaving stains on the surface, and the material is environmentally durable, has a high transmittance of about 90%, and is antithrombogenic. The results of this study suggest that this SLIPS may facilitate the creation of nonfouling medical devices through a low-cost, eco-friendly, and simple process.

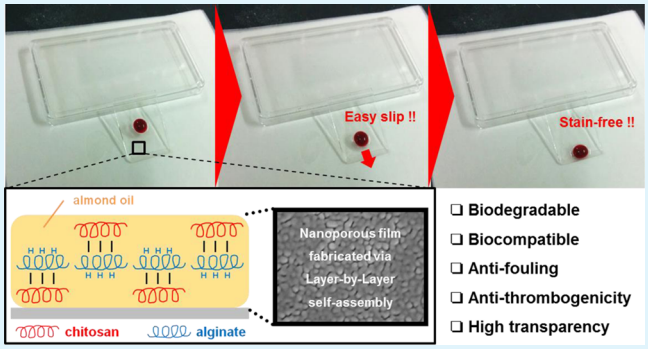

KEYWORDS: *slippery liquid-infused porous surface, SLIPS, layer-by-layer, biomimetic, antifouling, biocompatibility, antithrombogenic*

INTRODUCTION

Over the past decade, endoscopic surgery has become popular as a minimally invasive approach.[1] Although endoscopic surgery is enabled by visualization through the endoscope lens, low visibility of the image caused by blood staining on its surfaces remains a large problem.[2] The endoscope must be cleaned several times during each operation to remove blood and biological fluids from the endoscopic lens, which has the potential to increase the risk of blood clots and cause foreign material interfusion by the blood solidifying on the surface.[3,4] These complications increase surgical time, patient costs, and hospital medical expenses, among other problems. Additional medical devices such as stents also require antifouling surfaces. Stents have been widely used for the treatment of coronary artery disease, wherein the stent is inserted into a blood vessel, and expanded, restoring blood flow to the artery by pressing the atheromatosis onto the vascular wall.[5] Although drug-eluting stents have the potential to lyse blood clots,[6] there is no lasting effect after all of the drug has been eluted and it increases the risk of in-stent restenosis and atherosclerotic formation. Therefore, there is a critical need for the development of an antifouling coating that can prevent the formation of blood clots, atherosclerosis, clot accumulation, and restenosis.

In the field of antifouling surface materials, there has been a large amount of discussion focused on using biomimetic surfaces[7−9] such as mosquito eyes,[10,11] lotus leaves,[12,13] and shark skin.[14,15] The properties of these example biological tissues are determined by their micro/nanoarchitecture, which generates liquid−air and solid−air interfaces.[16,17] In particular, a number of research groups have been studying the preparation of superhydrophobic surfaces that mimic lotus leaves by combining an appropriate surface roughness with micro/nano hierarchical structures and materials with low surface energy. These materials demonstrate excellent properties, including being self-cleaning,[18] antifouling,[19] antifrosting,[20] and anti-icing,[21] which are applicable both for pure scientific interest and industrial applications. Despite a considerable amount of effort, however, it remains difficult to produce blood-repellent surfaces that are antithrombogenic.[22]

One of the biomimetic designs for creating an antifouling super-repellent surface was inspired by *Nepenthes*, the pitcher plant.[23,24] This material was named a slippery liquid-infused

Received: December 3, 2014
Accepted: February 3, 2015
Published: February 3, 2015

DOI: 10.1021/am508393n
ACS Appl. Mater. Interfaces 2015, 7, 4763−4771

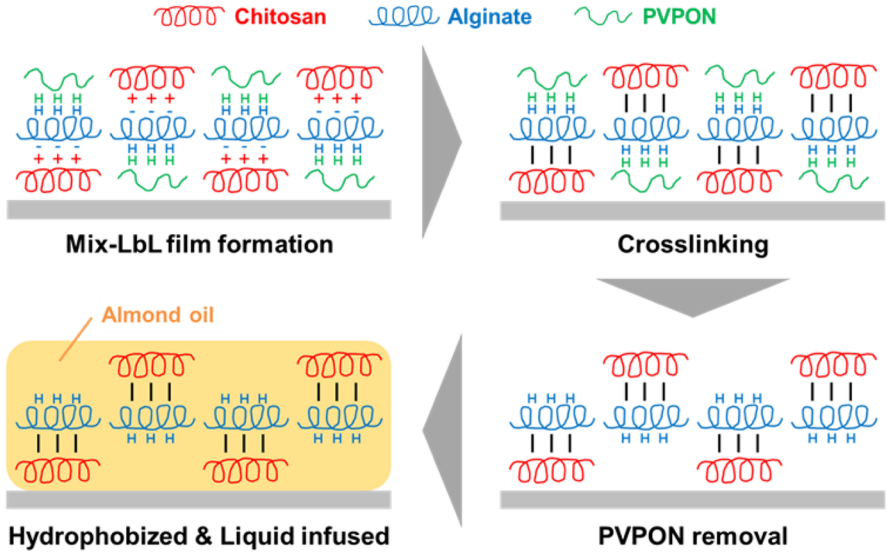

Figure 1. Schematic diagram showing the fabrication procedure for a biodegradable and biocompatible nonfluorinated SLIPS.

porous surface (SLIPS) and was composed of a hydrophobized porous underlayer and lubricant oil. The porous membrane, with its nanotopography and low surface energy, allowed the infused lubricating fluid to stick to it, forming a stable, defect-free, and inert slippery interface.[25,26] Therefore, to develop other SLIPS, the underlayer and lubricant oil should be carefully selected depending on the intended use. Two examples of changing the underlayer were reported by our group, including a gel-SLIPS fabricated by a facile nanoscale phase separation method[27] and an antireflective-SLIPS with transmittance of 97% produced using a layer-by-layer (LbL) self-assembly method.[28]

Decher et al. first used LbL self-assembly to fabricate multilayer thin films in the early 1990s.[29] LbL self-assembly is based on the alternating adsorption of oppositely charged polyelectrolytes via electrostatic attraction. It is a low-cost, eco-friendly, and simple tool to build up multilayer films with tailored nanosize structures.[30] There are few limitations in terms of substrates and components that can be used with LbL.[31] Although electrostatic interactions have been widely used to create multilayer films, other weaker interactions, such as hydrogen-bonding, have also been used as the driving force for the LbL self-assembly.[32] Hydrogen-bonding LbL assembly was first demonstrated by Rubner et al. and Zhang et al. simultaneously in 1997.[33,34] Hydrogen-bonding LbL films are created by the alternating deposition of polymers with a hydrogen bond acceptor and a hydrogen bond donor.[35] Hydrogen-bonding LbL films are more difficult to create than electrostatically assembled films.[36] However, they offer new possibilities for certain applications. Hydrogen-bonding assembly offers three major advantages. First, it allows the easy production of thin films that are responsive to pH.[37,38] Second, there are many methods for converting hydrogen-bonding films into single- or multicomponent ultrathin hydrogel materials.[39,40] Third, it permits the inclusion of polymers with low glass transition temperatures within the thin films.[41,42] These properties open up many novel applications of LbL self-assembled films, such as pH- or temperature-responsive drug delivery systems,[43,44] materials with tunable mechanical properties, and films dissolvable under physiological conditions,[45,46] among others.

As mentioned above, it has been often discussed that various underlayers could be used with functionalized SLIPS.[47,48] However, to the best of our knowledge, most reported SLIPS have consisted of fluorinated lubricant oils such as perfluoropolyether and few studies have investigated other lubricant fluid options.[49] Moreover, this previous work that fabricated fluorinated SLIPS composed of a fluorinated underlayer and oil are not biocompatible.[50,51] Therefore, the aim of the present study was on developing a nonfluorinated SLIPS with biodegradable and biocompatible materials using the experimental procedure shown in Figure 1. The underlayer was built up with chitosan, sodium alginate, and polyvinylpyrrolidone (PVPON) via the electrostatic and hydrogen-bonding LbL self-assembly methods.[37,52] To create porosity in the structure, the PVPON was removed by immersing the cross-linked chitosan and alginate film in a buffer solution at pH 10, making use of the pH-sensitivity of hydrogen bonds. After methyl silanization with decyltrimethoxysilane (DTMS), the film surface was covered with biocompatible almond oil, which is used as the main raw material in surgical bone wax, cosmetic oil, and so on.[53] Especially, sweet almond oil is safe on the basis of clinical experience.[54] The DTMS is not hazardous, and inducing hydrophobicity with methyl groups should have a smaller impact on the human body than fluorine components, which are nonbiodegradable, high cost, easily react with other materials, and impede the nerve growth in children after environmental exposure.[55] We demonstrated the feasibility of using nonfluorinated almond oil to stick to the porous underlayer of the SLIPS based on the surface energy in changing from fluorinated oil to nonfluorinated fluid. Further, this biodegradable and biocompatible SLIPS, which is stable under physiological conditions, was investigated to determine whether it could be applied to medical devices, such as endoscopes and stents, by measuring the optical properties and film thickness as fundamental characteristic of the thin film, as well as its ability to repel liquid and the blood coagulation time.

EXPERIMENTAL SECTION

Materials. Chitosan (chitosan-10, Wako Pure Chemical Industries, Ltd., Osaka, Japan), sodium alginate (Nacalai Tesque, Inc., Kyoto, Japan), PVPON (MW ~55 kDa, Sigma-Aldrich, St. Louis, MO, USA), 1-ethyl-3-(3-(dimethylamino)propyl) carbodiimide (EDC) (Wako

DOI: 10.1021/am508393n
ACS Appl. Mater. Interfaces 2015, 7, 4763−4771

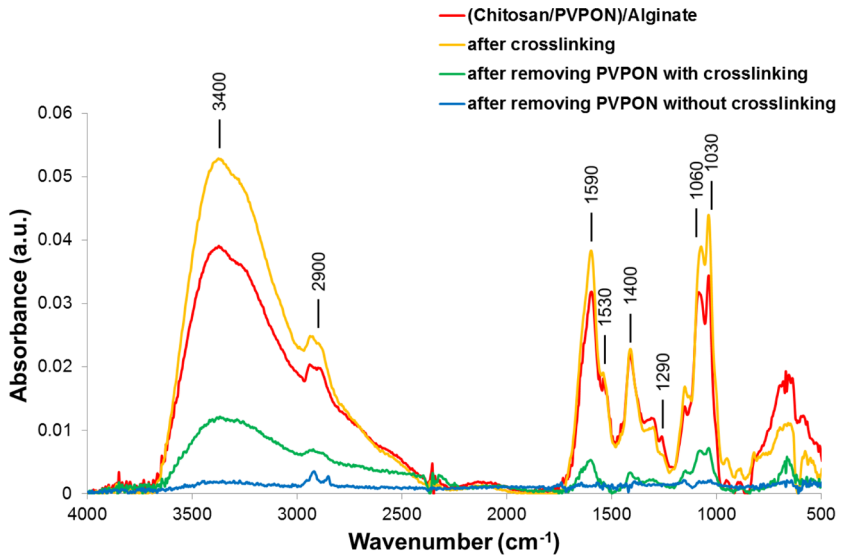

Figure 2. FT-IR spectra of the precursor (Chitosan/PVPON)/Alginate film (red line), a cross-linked film (orange line), a porous film after removing PVPON from the cross-linked film (green line), and a film after removing PVPON from a non-cross-linked film (blue line).

Pure Chemical Industries, Ltd., Osaka, Japan), ethanol (EtOH) (Kanto Chemical Co., Inc., Tokyo, Japan), HCl (Kanto Chemical Co., Inc., Tokyo, Japan), decyltrimethoxysilane (DTMS) (Shin-Etsu Chemical Co., Ltd., Tokyo, Japan), sweet almond oil (Original Co., Ltd., Tokyo, Japan), and glass substrates (76 × 26 mm; thickness, 1.0 mm; refractive index, 1.52; Matsunami Glass Ind., Ltd., Kishiwada, Japan) were used to produce the films. A 10 mM buffer solution at pH 4 was prepared from acetic acid (Kanto Chemical Co., Inc., Tokyo, Japan), sodium acetate, and ultrapure water (Aquarius GS-500.CPW, Advantec Co., Saijo, Japan). A 10 mM buffer solution at pH 10 was prepared from Na_2CO_3, Na_2HCO_3, (Wako Pure Chemical Industries, Ltd., Osaka, Japan), and ultrapure water. All polyelectrolyte dipping solutions were fabricated using the acetate buffer solution at pH 4. The glass substrates were cleaned in KOH (Junsei Chemical Co., Ltd., Tokyo, Japan) solution (1:120:60 wt % of KOH:H_2O:ethanol) for 2 min, and then rinsed thoroughly with ultrapure water before use.

Precursor Film Preparation. Appropriate precursor films were prepared for the formation of the porous underlayer by assembling sodium alginate and alternating with a mixture of a polyelectrolyte (chitosan) and hydrogen-bonding polymer (PVPON), a procedure that we refer to as mix-LbL. The glass substrate was immersed in the chitosan/PVPON mixture (1 mg/mL; vol % of 25:75, 50:50, or 75:25) for 10 min, and then rinsed three times in buffer solution for a total of 3 min. Next, the substrate was immersed in sodium alginate solution (1 mg/mL) for 10 min and then also rinsed with buffer solution. This dipping cycle corresponds to the deposition of one bilayer. The cycle was repeated until the desired number of bilayers was reached. The pH of all the solutions used to build up the film was adjusted to 4. The films were fabricated with an automatic LbL fabrication machine (Nano Film Maker, SNT Co., Kawasaki, Japan). The films were dried after multilayer assembly under a gentle stream of nitrogen gas.

Cross-Linking. The 20 bilayer blended precursor films of (Chitosan/PVPON)/Alginate were cross-linked in EDC solution (pH 5, 200 mM EDC in 50:50 vol % EtOH:H_2O) for 24 h at 4 °C to form amide bonds between the chitosan and alginate. The films were then rinsed twice for 5 min in a solution adjusted to pH 5 by adding HCl.

PVPON Removal. To remove the hydrogen-bonding component (PVPON) from the cross-linked LbL films, the films were immersed in buffer solution (pH 10, 10 mM Na_2CO_3/Na_2HCO_3 in 50:50 vol % EtOH:H_2O) for 2 h, and then rinsed twice for 5 min in pure water.

Hydrophobizing and Liquid Infusing. The porous multilayer films (chitosan:PVPON, vol % of 50:50) were hydrophobized via the gas phase method by placing it in a 100 mL glass bottle along with a 2 mL glass bottle containing DTMS (200 μL). The system was placed in a thermal incubator for 2.5 h at 140 °C. The almond oil (1 μL cm^{-2}) was added dropwise onto the hydrophobized film. Excess almond oil on the films was removed by blowing the surface with nitrogen gas.

Blood Coagulation Test. The coagulation of blood (3 μL of pig blood with 0.3 wt % citric acid, Tokyo Shibaura Zouki Co., Tokyo, Japan) on glass, the porous chitosan/alginate film after PVPON removal, the hydrophobized porous film, and biocompatible SLIPS was observed by digital microscopy (VHX-1000, Keyence, Osaka, Japan). The time point at which the blood showed no fluidity and changed color because of clotting was used as the blood coagulation time.

Characterization. The chemical bonds within the films before and after cross-linking and PVPON removal on plasma-treated silicon substrates were examined by Fourier transform infrared spectroscopy (FT-IR) (ALPHA-T, Bruker, Billerica, MA, USA), based on the related study.[56] Field emission scanning electron microscopy (FE-SEM, S-4700, Hitachi, Tokyo, Japan) images were taken with an accelerating voltage of 3 kV to characterize the surface nanotopography of the films. The film thickness and refractive index of the thin films coated on the glass substrates were determined by ellipsometry (MARY-102, Five Lab Co., Saitama, Japan). Transmittance in the spectral range from 300 to 1000 nm was measured by a spectrophotometer (UVmini-1240, Shimadzu, Kyoto, Japan). The contact angles and sliding angles for a 5 μL droplet were measured using a contact-angle meter (CA-DT, Kyowa, Tokyo, Japan). Surface tension measurements were made by a fully automatic surface tensiometer (CBVP-Z, Scientific Gear, Fairfax, VA, USA). The total transmittance was measured by a haze meter (NDH-5000, Nippon Denshoku Industries, Co., Ltd., Tokyo, Japan) with a white light-emitting diode (5 V, 3 W) as the optical source.

RESULTS AND DISCUSSION

The FT-IR analyses performed on the (Chitosan/PVPON)/Alginate film before and after EDC treatment showed an increase in both amide bands (amide I, 1590 cm^{-1}; amide II, 1530 cm^{-1}), as can be seen in Figure 2. This result indicated that the cross-linking reaction between the amine groups of chitosan and carboxylic groups of alginate was successful. From the FT-IR spectra of each powder (chitosan, PVPON, and sodium alginate, Supporting Information Figure S1), we determined that the peaks at around 1290 cm^{-1} were derived from C−H stretching vibration of PVPON, and those around 1060, 1400, and 1590 cm^{-1} were derived from asymmetrical

DOI: 10.1021/am508393n
ACS Appl. Mater. Interfaces 2015, 7, 4763−4771

C−O−C, symmetrical O−C−O, and asymmetrical O−C−O stretching vibration of chitosan and sodium alginate, respectively. After cross-linking in EDC solution at pH 5, 1290 cm^{-1} of the PVPON peak was slightly decreased because of the loss of hydrogen bonds between PVPON and alginate caused by the increased pH.

To confirm the removal of PVPON from the cross-linked film and the film stability, the IR peaks of the cross-linked or non-cross-linked films were measured after being dipped in buffer solution at pH 10. After the pH of the cross-linked filmwas increased, although 1290 cm^{-1} of the PVPON peak completely disappeared, several major peaks remained, corresponding to each stretching vibration mode of the amide bands, chitosan, and alginate. Conversely, after PVPON was removed from the non-cross-linked film, all of the peaks completely disappeared, indicating that cross-linking of the film was necessary and made it resistant to pH changes. In addition, XPS analysis was conducted to support FT-IR results and prove the existence of the films after removing PVPON by immersing them into pH 10 buffer solution (Supporting Information Figure S2).

As shown in the SEM images in Figure 3, the film structure of the precursor (Chitosan/PVPON)/Alginate film and the cross-linked film were nearly flat because multilayers consisting of similarly structured biomacromolecules tend to be flat, showing no topography or aggregation. The removal of PVPON created an orderly nanotopography and porosity (Supporting Information Figures S3 and S4). As also found in a related study by Caruso et al.,[39] PVPON removal can produce regular nanopores in the films because they were constructed from the self-assembly of a PVPON and chitosan polymer mixture solution and an alginate solution, which together formed energetically stable structures.[22]

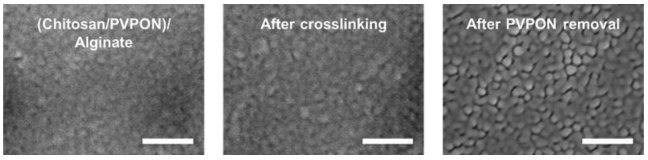

Figure 3. FE-SEM images of the precursor (Chitosan/PVPON)/Alginate film (left), a cross-linked film (center), and a porous film after PVPON removal from the cross-linked film (right). Scale bars: 300 nm.

The ellipsometry analysis (Figure 4) also suggested an increase in porosity after PVPON removal. According to the Fresnel equations, the refractive index of a LbL film can be estimated using a simple mixing rule:[57]

$$n_l = f_{air} n_{air} + f_{polyelectrolyte1} n_{polyelectrolyte1} + f_{polyelectrolyte2} n_{polyelectrolyte2} \quad (1)$$

where f_x is the volume fraction and n_x is the refractive index of component x. According to this equation, a decrease in the refractive index of LbL films is equal to an increase in their porosity. Indeed, we found that the magnitude of the decrease in the refractive index after removing PVPON depended on the PVPON content in the mixed solution of chitosan and PVPON. The refractive index decreased further as the PVPON content ratio increased because dipping the film in buffer solution at pH 10 created empty spaces in place of the physical space occupied by the PVPON.

The film thickness also depended on the PVPON content ratio. As the mixture solution PVPON ratio decreased, which was equal to an increase in the chitosan ratio, the film thicknesses increased because the electrostatic interactions between chitosan and alginate are stronger than the hydrogen-bonding interactions between PVPON and alginate and can promote film growth (Supporting Information Figure S5). After PVPON was removed, the thickness of all films was decreased because the multilayers also shrank as the PVPON was removed from the cross-linked films in buffer solution at pH 10. After the chitosan:PVPON vol % 25:75 film was dipped, however, the film partially detached from the glass substrate. Therefore, we used the (Chitosan/PVPON)/Alginate precursor film made from chitosan:PVPON vol % of 50:50 for the following experiments.

The films showed increased film thickness and refractive index after the hydrophobization treatment for 2.5 h at 140 °C, which caused film swelling derived from the evaporation of small amounts of moisture contained in the multilayer.[28] Multilayer films fabricated using LbL with water-soluble

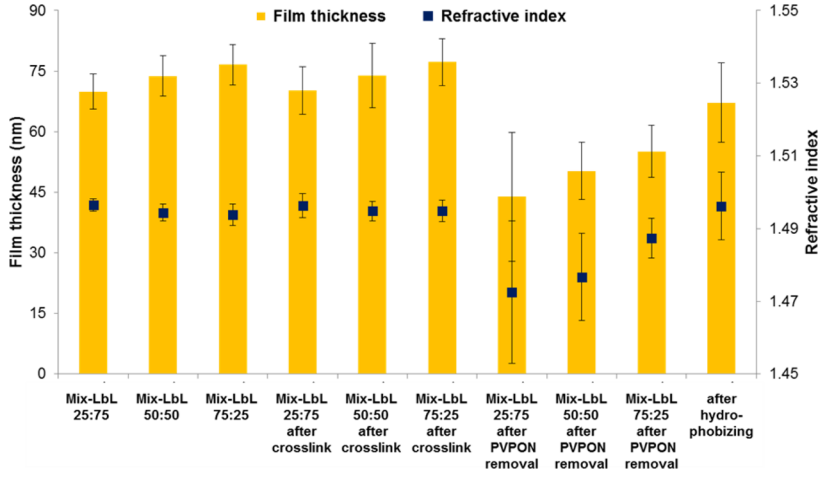

Figure 4. Film thickness (yellow bars) and refractive index (blue squares) of the precursor (Chitosan/PVPON)/Alginate films made with different mixture fractions (chitosan:PVPON vol % of 25:75, 50:50, and 75:25), cross-linked films, porous films after PVPON removal from the cross-linked films, and hydrophobized porous films (chitosan:PVPON, vol % of 50:50) by ellipsometry. Mix-LbL X:Y indicates precursor (Chitosan/PVPON)/Alginate films and their mixture fraction.

DOI: 10.1021/am508393n
ACS Appl. Mater. Interfaces 2015, 7, 4763−4771

polymers first swell, and then shrink and cure after applying heat because of the impermeable polymer substrate.

Changes in the light transmittance of the films are shown in Figure 5. The presence of the films decreased the difference in refractive index between the glass substrate and air,[28] and the transmittance of the (Chitosan/PVPON)/Alginate films became higher than that of the glass substrate. Although the transmittance was maintained after cross-linking, the transmittance of the porous film after removing PVPON was decreased because of an increase in light scattering caused by the porosity and nanotopography of the films, as assessed with FE-SEM images. The hydrophobized porous films showed the lowest transmittance because their refractive index and scattering structure were higher than those of the porous film before hydrophobization. After dropping the almond oil onto the hydrophobized porous films to create the biodegradable and biocompatible SLIPS, the transmittance was increased because of the increased parallel transmittance and decreased diffusion (Supporting Information Figure S6). This indicates that light scattering caused by the surface topography and the difference in refractive index at the solid−gas interface both decreased after the application of almond oil.

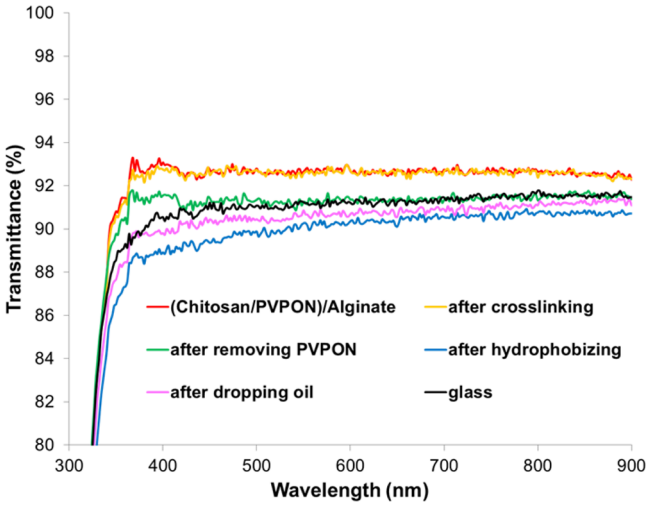

Figure 5. Changes in the transmittance of the films. The transmittance of the glass substrate (black line), a precursor (Chitosan/PVPON)/Alginate film (chitosan:PVPON vol % of 50:50, red line), a cross-linked film (yellow line), a porous film after removing PVPON from the cross-linked film (green line), a hydrophobized porous film (blue line), and a biocompatible SLIPS after dropping oil onto the hydrophobized porous film (pink line) on glass substrates with air as the background.

The hydrophobization treatment changed the surface from hydrophilic to hydrophobic as shown in Figure 6. Before hydrophobization, the contact angles on the hydrophilic films were close to zero because of their hydrophilicity and absorption of the water-soluble polymers (Supporting Information Figure S7). The contact angles of water and almond oil on the hydrophobic films were measured to determine whether the hydrophobized porous films met the following criteria of SLIPS:[23]

$$\Delta E_1 = \gamma_{oa}\cos\theta_o - \gamma_{wa}\cos\theta_w - \gamma_{wo} > 0 \quad (2)$$

$$\Delta E_2 = \gamma_{oa}\cos\theta_o - \gamma_{wa}\cos\theta_w + \gamma_{wa} - \gamma_{oa} > 0 \quad (3)$$

where γ_{xy} is the interfacial tension between the two phases designated by subscripts w (water), o (almond oil), and a (air). θ_o and θ_w are the contact angles of almond oil and water on the hydrophobic multilayer in the presence of air. γ_{wo} was calculated using Fowkes equation:[23]

$$\gamma_{wo} = \gamma_{oa} + \gamma_{wa} - 2(\gamma_{oa}^{\alpha}\gamma_{wa}^{\alpha})^{1/2} \quad (4)$$

where γ_{oa}^{α} and γ_{wa}^{α} are the dispersion force contributions of the liquid surface tensions. The dispersion force contribution of water the surface tension was 21.8 mN/m. For nonpolar materials, $\gamma_{oa}^{\alpha} \approx \gamma_{oa}$.[21]

After hydrophobization, the films did not achieve superhydrophobicity because they demonstrated nanotopography, but not microtopography, as mentioned in the introduction. The hydrophobic porous surface met the criteria for SLIPS and displayed a stable liquid surface, as described in Table 1, indicating that this film was a SLIPS with a biodegradable

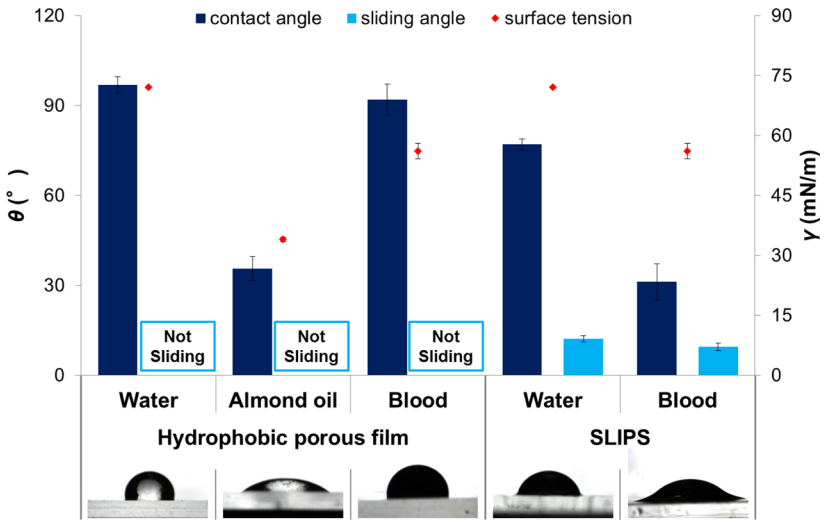

Figure 6. Contact angle (dark blue bars), sliding angle (light blue bars), and surface tension (red diamonds) of water, almond oil, and blood on a hydrophobized porous film and on a biocompatible SLIPS, made by dropping oil onto a hydrophobized porous film. Below: corresponding photographic images of each liquid drop on the different films.

DOI: 10.1021/am508393n
ACS Appl. Mater. Interfaces 2015, 7, 4763−4771

Table 1. Measured Contact Angles and Surface Tensions of Water and Almond Oil, and the Calculated Interfacial Tension and Spreading Coefficient between Water and Almond Oil

water			almond oil						
γ_{wa} (mN/m)	θ_w (deg)	γ^{α}_{wa} (mN/m)	γ_{oa} (mN/m)	θ_o (deg)	γ^{α}_{oa} (mN/m)	γ_{wo} (mN/m)	ΔE_1	ΔE_2	$S_{ow(a)}$
72.1	97	21.8	34	35.7	34	51.7	1.71	91.5	−13.6

porous underlayer made using a biocompatible, nonfluorinated fluid.

Although the water droplet did not slide on the hydrophobic multilayer, the biodegradable and biocompatible SLIPS showed a low sliding angle of water at approximately 10°.

The criterion for cloaking is determined by the spreading coefficient as[58]

$$S_{ow(a)} = \gamma_{wa} - \gamma_{wo} - \gamma_{oa} \quad (5)$$

$S_{ow(a)} > 0$ implies that the water droplet will be cloaked by the lubricant fluid and that the lubricant can be easily lost through evaporation, whereas $S_{ow(a)} < 0$ implies that the water droplet will not be cloaked by the lubricant fluid and that the lubricant will remain stuck in the porous underlayer without evaporating. For the biodegradable and biocompatible SLIPS, $S_{ow(a)} = -13.6$ (Table 1), which indicated that the lubricant fluid encapsulating the porous multilayer was stable. Indeed, the biodegradable and biocompatible SLIPS continued to perform as a SLIPS with a water sliding angle of less than 25° and total transmittance of more than 85% after exposure for 1−30 days at room temperature (Figure 7). Although the sliding angle was slightly

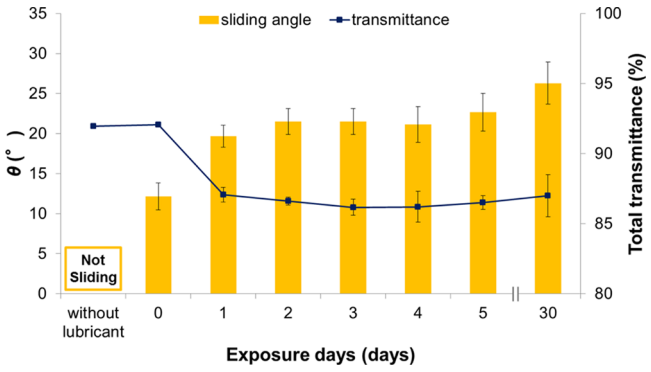

Figure 7. Changes in the water sliding angles (yellow bars) and total transmittance (blue squares) of a biocompatible SLIPS after increasing days of exposure at room temperature. The total transmittance, which is the sum of parallel transmittance and forward diffusion, was measured using a haze meter.

increased and transmittance was slightly decreased after 1 day of exposure, only small changes in both properties were found after further exposure, suggesting that after 1 day of exposure, the evaporation of almond oil was minimal and a stable lubricant layer remained.

As another durability test for practical use, the robustness of biocompatible SLIPS was investigated by subjecting it to high shear and comparing sliding angle of water and blood in air using a spin coater at different spinning speeds (Supporting Information Figure S8).[25] After the shear test from 250 to 6000 rpm, the SLIPS maintained the repellency. In addition, to test the stability of biocompatible SLIPS in fluid, sliding angles of water and blood after exposing under running water for different water flowing time were measured (Supporting Information Figure S9). The films maintained the repellency until 4 h exposure. However, the sliding angle of both liquid continued to increase, and blood did not slide after 9 h, and water did not slide after 11 h.

Antithrombogenic Properties. Finally, the time to achieve blood coagulation on each film was determined through observation using a digital microscope (Figure 8). The glass substrate was used as a reference, and blood on the glass coagulated in 12 min. Blood coagulation on the porous multilayer before hydrophobization occurred in 8 min because of the blood-clotting functions of chitosan and alginate. In contrast, the blood coagulation time was increased on the hydrophobized porous multilayer and biocompatible SLIPS. The DTMS applied to the hydrophobized film created a surface with low surface energy and prevented blood from attaching to the chitosan and alginate. Interactions between artificial material surfaces and blood are known to occur by using adsorbed blood proteins as the intermediary.[22,24] Therefore, the adsorption of proteins was likely blocked on the hydrophobized multilayer, giving the film its anticoagulation property. The biocompatible SLIPS demonstrated significant antithrombogenicity caused by its low surface wettability and the anticoagulation property of almond oil, whose main component is oleic acid. Oleic acid enhances the antithrombin activity of the film by binding to lysine residues near the N-terminus of antithrombin III, which is a physiological serine protease inhibitor that controls the coagulation reaction as a blood clotting inhibitor and promotes reactions with the serine proteolytic enzymes.[59] Linoleic acid, another major component of almond oil, is incorporated into lipoprotein lipids and demonstrates an antiatherogenic effect. The enrichment of lipoprotein particles with less oleic acid at the expense of linoleic acid increases their resistance to oxidative stress because of the increased susceptibility to oxidation of lipoproteins enriched with linoleic acid, reducing platelet activity.[60] Moreover, the evaporation of blood was prevented at the interface between the blood and lubricant oil by covering the edge of the target liquid with lubricant fluid (Figure 6). Although the blood on the biocompatible SLIPS coagulated after 30 min, the clotted blood was easily repelled and removed from the surface without leaving a stain (Supporting Information Figure S10). In addition, the sliding angles of the blood on the hydrophobic surface and the biocompatible SLIPS were measured (Figure 6). The surface tension of the blood was lower than that of water by 15 mN/m. As described in a previous study, lower surface tensions were associated with lower sliding angles on the SLIPS.[27,28] In the present study, blood was easily repelled from the biocompatible SLIPS compared with water because of the increased mobility of the lubricant layer.[27,28] After the blood flowed off the film, no stain or trace from the flow of blood remained (Supporting Information Figure S11). Together, these results indicated that the biodegradable and biocompatible SLIPS was stable under physiological conditions and was the most appropriate coating film, compared with bare glass, the porous LbL multilayer, and the hydrophobized porous multilayer, for use in various medical coating applications.

DOI: 10.1021/am508393n
ACS Appl. Mater. Interfaces 2015, 7, 4763−4771

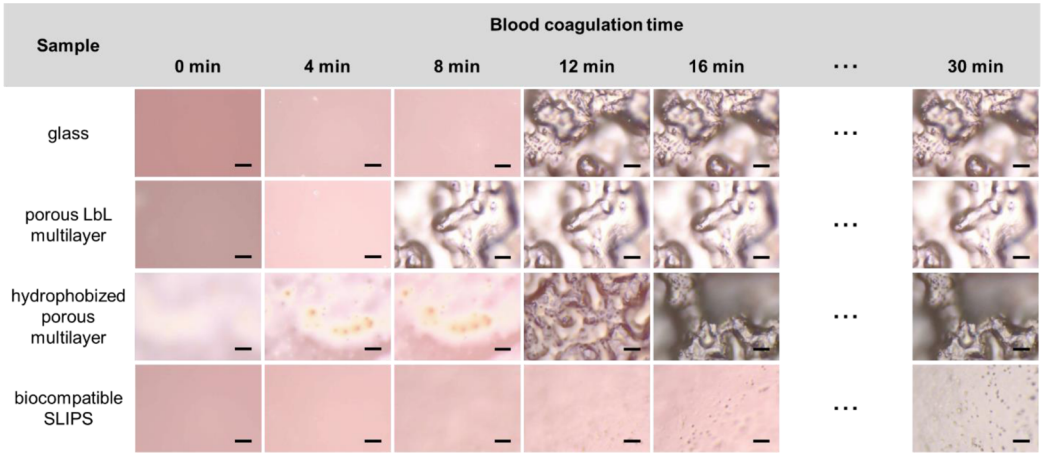

Figure 8. Time for blood coagulation on a glass substrate (first line), porous films after removing PVPON from a cross-linked film (second line), a hydrophobized porous film (third line), and a biocompatible SLIPS after dropping oil onto the hydrophobized porous film (fourth line), as imaged with a digital microscope. Scale bars: 10 μm.

CONCLUSIONS

We have demonstrated a nonfluorinated slippery liquid-infused coating based on a textured biodegradable polyelectrolyte multilayer and biocompatible plant oil. The underlayer was well cross-linked and stable at physiological conditions. The feasibility and stability of creating a nonfluorinated SLIPS covered with almond oil as the porous underlayer was theoretically explained based on surface energy, which indicated that almond oil and blood were immiscible. These materials repelled blood, indicating the antithrombogenicity of their surface, which also delayed the blood coagulation time compared with other coatings with different surface wettability. In addition, the material was durable in the environment for 30 days, maintaining a transmittance of approximately 90%. This film was constructed using a low-cost, eco-friendly, and simple LbL method that can be applied to the coating of curved surfaces, regardless of the radius of curvature. This biocompatible SLIPS, consisting of both a biocompatible underlayer and biocompatible lubricant fluid, may be able to sustain its properties during surgical use for longer than a few hours. The creation of a stable nonfluorinated oil surface on a porous membrane may also contribute to a better understanding of the fluid-infused surface. Although the mechanical properties and stability, such as abrasion resistance, remain to be determined as future challenges, such further study of biodegradable and biocompatible SLIPS would also be valuable to the field of antifouling surfaces for new medical applications, including for endoscopes and stents.

ASSOCIATED CONTENT

Supporting Information

FT-IR spectra of chitosan, polyvinylpyrrolidone and sodium alginate powders, XPS analysis of precursor film, cross-linked film, cross-linked- and non-cross-linked film after removing PVPON, AFM images, FE-SEM image with low magnification, film growth, measurement results of total transmittance, parallel transmittance, diffusion and haze values, CCD camera images of blood droplet on each surface, film stability after spinning film stability under running water, blood removability on biocompatible SLIPS, and photo images of blood repellency on biocompatible SLIPS. This material is available free of charge via the Internet at http://pubs.acs.org.

AUTHOR INFORMATION

Corresponding Author

*Seimei Shiratori. E-mail: shiratori@appi.keio.ac.jp.

Author Contributions

K.M. conceived, designed, and carried out the experiments, analyzed the data, and wrote the paper. K.-H.K. provided experimental support and support in data analysis. S.S. gave scientific advice and commented on the paper.

Notes

The authors declare no competing financial interest.

ACKNOWLEDGMENTS

We are deeply grateful to Dr. Kouji Fujimoto and Mr. Ken Suwabe, whose insightful comments and suggestions were of inestimable value for our study. We are indebted to Dr. Yoshio Hotta, whose meticulous comments were an enormous help.

REFERENCES

(1) Davis, C. J.; Filipi, C. J. A History of Endoscopic Surgery. In *Principles of Laparoscopic Surgery: Basic and Advanced Techniques*; Arregui, M. E., Fitzgibbons, R. J. Jr., Katkhouda, N., McKernan, J. B., Reich, H., Eds.; Springer: New York, 1995; pp 3−20.

(2) Harrel, S. K.; Wilson, T. G.; Rivera-Hidalgo, F. A Videoscope for Use in Minimally Invasive Periodontal Surgery. *J. Clin. Periodontol.* **2013**, *40*, 868−874.

(3) Kalra, G.; Keir, J.; Tahery, J. Prevention of Blood Staining of Endoscope Tip During Functional Endoscopic Sinus Surgery: Sleeve Technique. *J. Laryngol. Otol.* **2009**, *123*, 1358−1359.

(4) Dalke, K.; Mierzwiński, J.; Burduk, P. A Simple-Irrigating System for Endoscopic Sinus Surgery. *Otolaryngol. Polym.* **2005**, *60*, 187−189.

(5) Hennequin, L. M.; Joffre, F. G.; Rousseau, H. P.; Aziza, R.; Tregant, P.; Bernadet, P.; Salvador, M.; Chamontin, B. Renal Artery Stent Placement: Long-Term Results with the Wallstent Endoprosthesis. *Radiology* **1994**, *191*, 713−719.

(6) Deconinck, E.; Sohier, J.; De Scheerder, I.; Van den Mooter, G. Pharmaceutical Aspects of Drug Eluting Stents. *J. Pharm. Sci.* **2008**, *97*, 5047−5060.

(7) Liu, K.; Jiang, L. Bio-Inspired Self-Cleaning Surfaces. *Annu. Rev. Mater. Res.* **2012**, *42*, 231−263.

(8) Bhushan, B. Bioinspired Structured Surfaces. *Langmuir* **2012**, *28*, 1698−1714.

(9) Hirai, Y.; Yabu, H.; Matsuo, Y.; Ijiro, K.; Shimomura, M. Biomimetic Bi-Functional Silicon Nanospike-Array Structures Pre-

DOI: 10.1021/am508393n
ACS Appl. Mater. Interfaces 2015, 7, 4763−4771

pared by Using Self-Organized Honeycomb Templates and Reactive Ion Etching. *J. Mater. Chem.* **2010**, *20*, 10804−10808.
(10) Wu, F.; Shi, G.; Xu, H.; Liu, L.; Wang, Y.; Qi, D.; Lu, N. Fabrication of Antireflective Compound Eyes by Imprinting. *ACS Appl. Mater. Interfaces* **2013**, *5*, 12799−12803.
(11) Sun, Z.; Liao, T.; Liu, K.; Jiang, L.; Kim, J. H.; Dou, S. X. Fly-Eye Inspired Superhydrophobic Anti-Fogging Inorganic Nanostructures. *Small* **2014**, *10*, 3001−3006.
(12) Wang, X.; Liu, X.; Zhou, F.; Liu, W. Self-Healing Superamphiphobicity. *Chem. Commun.* **2011**, *47*, 2324−2326.
(13) Nishimoto, S.; Bhushan, B. Bioinspired Self-Cleaning Surfaces with Superhydrophobicity, Superoleophobicity, and Superhydrophilicity. *RSC Adv.* **2013**, *3*, 671−690.
(14) Chung, K. K.; Schumacher, J. F.; Sampson, E. M.; Burne, R. A.; Antonelli, P. J.; Brennan, A. B. Impact of Engineered Surface Microtopography on Biofilm Formation of *Staphylococcus aureus*. *Biointerphases* **2007**, *2*, 89−94.
(15) Carman, M. L.; Estes, T. G.; Feinberg, A. W.; Schumacher, J. F.; Wilkerson, W.; Wilson, L. H.; Callow, M. E.; Callow, J. A.; Brennan, A. B. Engineered Antifouling Microtopographies − Correlating Wettability With Cell Attachment. *Biofouling* **2006**, *22*, 11−21.
(16) Li, X. M.; Reinhoudt, D.; Crego-Calama, M. What Do We Need for a Superhydrophobic Surface? A Review on the Recent Progress in the Preparation of Superhydrophobic Surfaces. *Chem. Soc. Rev.* **2007**, *36*, 1350−1368.
(17) Marmur, A. The Lotus Effect: Superhydrophobicity and Metastability. *Langmuir* **2004**, *20*, 3517−3519.
(18) Ragesh, P.; Ganesh, V. A.; Nair, S. V.; Nair, A. S. A Review on "Self-Cleaning and Multifunctional Materials". *J. Mater. Chem. A* **2014**, *2*, 14773−14797.
(19) Ueda, E.; Levkin, P. A. Emerging Applications of Superhydrophilic-Superhydrophobic Micropatterns. *Adv. Mater.* **2013**, *25*, 1234−1247.
(20) Sohn, Y.; Kim, D.; Lee, S.; Yin, M.; Song, J. Y.; Hwang, W.; Park, S.; Kim, H.; Ko, Y.; Han, I. Anti-Frost Coatings Containing Carbon Nanotube Composite with Reliable Thermal Cyclic Property. *J. Mater. Chem. A* **2014**, *2*, 11465−11471.
(21) Guo, P.; Zheng, Y.; Wen, M.; Song, C.; Lin, Y.; Jiang, L. Icephobic/Anti-Icing Properties of Micro/Nanostructured Surfaces. *Adv. Mater.* **2012**, *24*, 2642−2648.
(22) Matsuda, M.; Shiratori, S. Correlation of Antithrombogenicity and Heat Treatment for Layer-by-Layer Self-Assembled Polyelectrolyte Films. *Langmuir* **2011**, *27*, 4271−4277.
(23) Wong, T. S.; Kang, S. H.; Tang, S. K.; Smythe, E. J.; Hatton, B. D.; Grinthal, A.; Aizenberg, J. Bioinspired Self-Repairing Slippery Surfaces with Pressure-Stable Omniphobicity. *Nature* **2011**, *477*, 443−447.
(24) Leslie, D. C.; Waterhouse, A.; Berthet, J. B.; Valentin, T. M.; Watters, A. L.; Jain, A.; Kim, P.; Hatton, B. D.; Nedder, A.; Donovan, K.; Super, E. H.; Howell, C.; Johnson, C. P.; Vu, T. L.; Bolgen, D. E.; Rifai, S.; Hansen, A. R.; Aizenberg, M.; Super, M.; Aizenberg, J.; Ingber, D. E. A Bioinspired Omniphobic Surface Coating on Medical Devices Prevents Thrombosis and Biofouling. *Nat. Biotechnol.* **2014**, *32*, 1134−1140.
(25) Kim, P.; Kreder, M. J.; Alvarenga, J.; Aizenberg, J. Hierarchical or Not? Effect of the Length Scale and Hierarchy of the Surface Roughness on Omniphobicity of Lubricant-Infused Substrates. *Nano Lett.* **2013**, *13*, 1793−1799.
(26) Vogel, N.; Belisle, R. A.; Hatton, B.; Wong, T. S.; Aizenberg, J. Transparency and Damage Tolerance of Patternable Omniphobic Lubricated Surfaces Based on Inverse Colloidal Monolayers. *Nat. Commun.* **2013**, *4*, 2176.
(27) Okada, I.; Shiratori, S. High-Transparency, Self-Standable Gel-SLIPS Fabricated by a Facile Nanoscale Phase Separation. *ACS Appl. Mater. Interfaces* **2014**, *6*, 1502−1508.
(28) Manabe, K.; Nishizawa, S.; Kyung, K.-H.; Shiratori, S. Optical Phenomena and Antifrosting Property on Biomimetics Slippery Fluid-Infused Antireflective Films via Layer-by-Layer Comparison with Superhydrophobic and Antireflective Films. *ACS Appl. Mater. Interfaces* **2014**, *6*, 13985−13993.
(29) Decher, G. Fuzzy Nanoassemblies: Toward Layered Polymeric Multicomposites. *Science* **1997**, *277*, 1232−1237.
(30) Shiratori, S. S.; Rubner, M. F. pH-Dependent Thickness Behavior of Sequentially Adsorbed Layers of Weak Polyelectrolytes. *Macromolecules* **2000**, *33*, 4213−4219.
(31) Wang, Y.; Angelatos, A. S.; Caruso, F. Template Synthesis of Nanostructured Materials via Layer-by-Layer Assembly. *Chem. Mater.* **2007**, *20*, 848−858.
(32) Yang, S.; Zhang, Y.; Zhang, X.; Xu, J. The Influence of pH on a Hydrogen-Bonded Assembly Film. *Soft Matter* **2007**, *3*, 463−469.
(33) Stockton, W. B.; Rubner, M. F. Molecular-Level Processing of Conjugated Polymers. 4. Layer-by-Layer Manipulation of Polyaniline via Hydrogen-Bonding Interactions. *Macromolecules* **1997**, *30*, 2717−2725.
(34) Wang, L.; Wang, Z.; Zhang, X.; Shen, J.; Chi, L.; Fuchs, H. A New Approach for the Fabrication of an Alternating Multilayer Film of Poly(4-vinylpyridine) and Poly(acrylic acid) Based on Hydrogen Bonding. *Macromol. Rapid Commun.* **1997**, *18*, 509−514.
(35) Zhang, Y.; Guan, Y.; Yang, S.; Xu, J.; Han, C. C. Fabrication of Hollow Capsules Based on Hydrogen Bonding. *Adv. Mater.* **2003**, *15*, 832−835.
(36) Kharlampieva, E.; Sukhishvili, S. A. Hydrogen-Bonded Layer-by-Layer Polymer Films. *J. Macromol. Sci., Polym. Rev.* **2006**, *46*, 377−395.
(37) Städler, B.; Price, A. D.; Chandrawati, R.; Hosta-Rigau, L.; Zelikin, A. N.; Caruso, F. Polymer Hydrogel Capsules: En Route toward Synthetic Cellular Systems. *Nanoscale* **2009**, *1*, 68−73.
(38) Sukhishvili, S. A.; Granick, S. Layered, Erasable Polymer Multilayers Formed by Hydrogen-Bonded Sequential Self-Assembly. *Macromolecules* **2002**, *35*, 301−310.
(39) Li, Q.; Quinn, J. F.; Caruso, F. Nanoporous Polymer Thin Films via Polyelectrolyte Templating. *Adv. Mater.* **2005**, *17*, 2058−2062.
(40) Zhu, Z.; Sukhishvili, S. A. Temperature-Induced Swelling and Small Molecule Release with Hydrogen-Bonded Multilayers of Block Copolymer Micelles. *ACS Nano* **2009**, *3*, 3595−3605.
(41) Kharlampieva, E.; Kozlovskaya, V.; Sukhishvili, S. A. Layer-by-Layer Hydrogen-Bonded Polymer Films: From Fundamentals to Applications. *Adv. Mater.* **2009**, *21*, 3053−3065.
(42) Kim, B. S.; Park, S. W.; Hammond, P. T. Hydrogen-Bonding Layer-by-Layer-Assembled Biodegradable Polymeric Micelles as Drug Delivery Vehicles from Surfaces. *ACS Nano* **2008**, *2*, 386−392.
(43) Schmidt, D. J.; Hammond, P. T. Electrochemically Erasable Hydrogen-Bonded Thin Films. *Chem. Commun.* **2010**, *46*, 7358−7360.
(44) Meng, F.; Zhong, Z.; Feijen, J. Stimuli-Responsive Polymersomes for Programmed Drug Delivery. *Biomacromolecules* **2009**, *10*, 197−209.
(45) Zelikin, A. N.; Quinn, J. F.; Caruso, F. Disulfide Cross-Linked Polymer Capsules: En Route to Biodeconstructible Systems. *Biomacromolecules* **2006**, *7*, 27−30.
(46) Zelikin, A. N.; Li, Q.; Caruso, F. Degradable Polyelectrolyte Capsules Filled with Oligonucleotide Sequences. *Angew. Chem., Int. Ed.* **2006**, *45*, 7743−7745.
(47) Sunny, S.; Vogel, N.; Howell, C.; Vu, T. L.; Aizenberg, J. Lubricant-Infused Nanoparticulate Coatings Assembled by Layer-by-Layer Deposition. *Adv. Funct. Mater.* **2014**, *24*, 6658−6667.
(48) Huang, X.; Chrisman, J. D.; Zacharia, N. S. Omniphobic Slippery Coatings Based on Lubricant-Infused Porous Polyelectrolyte Multilayers. *ACS Macro Lett.* **2013**, *2*, 826−829.
(49) Wilson, P. W.; Lu, W.; Xu, H.; Kim, P.; Kreder, M. J.; Alvarenga, J.; Aizenberg, J. Inhibition of Ice Nucleation by Slippery Liquid-Infused Porous Surfaces (SLIPS). *Phys. Chem. Chem. Phys.* **2013**, *15*, 581−585.
(50) Li, J.; Kleintschek, T.; Rieder, A.; Cheng, Y.; Baumbach, T.; Obst, U.; Schwartz, T.; Levkin, P. A. Hydrophobic Liquid-Infused Porous Polymer Surfaces for Antibacterial Applications. *ACS Appl. Mater. Interfaces* **2013**, *5*, 6704−6711.
(51) Xiao, L.; Li, J.; Mieszkin, S.; Di Fino, A.; Clare, A. S.; Callow, M. E.; Callow, J. A.; Grunze, M.; Rosenhahn, A.; Levkin, P. A. Slippery

DOI: 10.1021/am508393n
ACS Appl. Mater. Interfaces 2015, 7, 4763−4771

Liquid-Infused Porous Surfaces Showing Marine Antibiofouling Properties. *ACS Appl. Mater. Interfaces* **2013**, *5*, 10074−10080.
(52) Shenoy, D. B.; Antipov, A. A.; Sukhorukov, G. B.; Möhwald, H. Layer-by-Layer Engineering of Biocompatible, Decomposable Core-Shell Structures. *Biomacromolecules* **2003**, *4*, 265−272.
(53) Alegre, M.; Garcés, J. R.; Puig, L. Bone Wax in Dermatologic Surgery. *Actas Dermo-Sifiliogr.* **2013**, *104*, 299−303.
(54) Elder, R. L. Final Report on the Safety Assessment of Sweet Almond Oil and Almond Meal. *J. Am. Coll. Toxicol.* **1983**, *2*, 85−99.
(55) Choi, A. L.; Sun, G.; Zhang, Y.; Grandjean, P. Developmental Fluoride Neurotoxicity: A Systematic Review and Meta-Analysis. *Environ. Health Perspect.* **2012**, *120*, 1362−1368.
(56) Wang, B. L.; Ren, K. F.; Chang, H.; Wang, J. L.; Ji, J. Construction of Degradable Multilayer Films for Enhanced Antibacterial Properties. *ACS Appl. Mater. Interfaces* **2013**, *5*, 4136−4143.
(57) Tan, W. S.; Du, Y.; Luna, L. E.; Khitass, Y.; Cohen, R. E.; Rubner, M. F. Templated Nanopores for Robust Functional Surface Porosity in Poly(methyl methacrylate). *Langmuir* **2012**, *28*, 13496−13502.
(58) Smith, J. D.; Dhiman, R.; Anand, S.; Reza-Garduno, E.; Cohen, R. E.; McKinley, G. H.; Varanasi, K. K. Droplet Mobility on Lubricant-Impregnated Surfaces. *Soft Matter* **2013**, *9*, 1772−1780.
(59) Mandl, J.; Tanács, B.; Spolarics, Z.; Garzó, T.; Mucha, I.; Antoni, F.; Machovich, R.; Horváth, I. Uptake of Arachidonic Acid, Arachidic Acid, Oleic Acid and Their Incorporation into Phospholipids and Triacylglycerols of Isolated Murine Hepatocytes. Effect of Thrombin-Antithrombin III Complex. *Thromb. Res.* **1984**, *35*, 407−414.
(60) Ros, E.; Mataix, J. Fatty Acid Composition of Nuts - Implications for Cardiovascular Health. *Br. J. Nutr.* **2006**, *96*, S29−S35.

DOI: 10.1021/am508393n
ACS Appl. Mater. Interfaces 2015, 7, 4763−4771